




## Automated true triaxial apparatus development for soil mechanics investigation

Dionatas Hoffmann Andreghetto<sup>1#</sup> , Lucas Festugato<sup>2</sup> ,  
Gustavo Dias Miguel<sup>2</sup> , Andressa da Silva<sup>2</sup> 

Article

### Keywords

True triaxial apparatus  
Soil stabilization  
Cemented fine sand  
Triaxial tests

### Abstract

Soil mechanical fully understanding requires considering a three dimensional approach, including soil response under the second principal stress and its potential anisotropy. In order to achieve such soil mechanical understanding, a true triaxial apparatus might be used. Therefore, in the present research an automated true triaxial apparatus was developed comprising its cubical cell, data acquisition and stress control systems. The manufactured apparatus was validated by means a laboratory test campaign where true triaxial test responses were compared to standard drained triaxial tests. True triaxial and standard drained triaxial tests were carried out on both naturally and artificially cemented soils. Results were gathered and compared. A soil mechanical compatibility was observed when test results of the newest true triaxial equipment were compared to test results obtained from a well validated standard triaxial apparatus. Thereby, the present paper reports an affordable successful true triaxial apparatus development demonstrating its efficiency for regular soil mechanical tests. Finally, a full stress rosette was established for a uniform fine sand where some small anisotropy was detected.

## 1. Introduction

The true triaxial apparatus (TTA) was developed to study the influence of the second normal stress on soil and rock samples and can be divided in three main types according to the boundaries state conditions. Among the possibilities, the soil sample-pressure interface might be rigid or flexible, as well as a mix between rigid and flexible boundaries may also be used. Hambly (1969) reported a rigid boundary true triaxial development, which consisted of a cubic chamber composed by six metal plate faces. Metal plate faces were driven by mechanical transducers and were responsible to apply displacements to the soil samples located in the cubic chamber core. The rigid plate faced TTA type are in general characterized to be a strain-controlled apparatus, where rigid plate faces incrementally apply strains on the soil or rock samples, thence, the three principal stresses might be in fact described as response variables. Strain-controlled TTA is indicated to investigate samples post peak behavior, which might be seen in most of the geotechnical apparatuses, such as standard triaxial (ST), direct simple shear and hollow cylinder devices. Nonetheless, some concerns have risen regarding strain-controlled TTA apparatus, namely, the equipment inability to apply uniform stresses on each sample

face, which may lead to stress concentration in some sample points. Strain-controlled TTA apparatuses can be found in several works such as Airey & Wood (1988), Ibsen & Praastrup (2002), Matsuoka et al. (2002) and Ismail et al. (2005). Alternatively, a flexible boundary TTA type can also be implemented, being them stress-controlled apparatus and, thus, having the main advantage of uniform stress application. In this type of TTA the principal stresses are applied by a flexible intermediating medium such as rubber membranes also known as cushions, which are responsible to create the sample-pressure interface. The flexible boundary TTA type is also found in numerous works such as Ko & Scott (1967), Sture & Desai (1979), Sivakugan et al. (1988), Reddy et al. (1992), Sadek (2006) and Choi et al. (2008). Finally, the last possibility concerns the combination of both rigid and flexible designs, which results in a mixed or hybrid TTA type. Therefore, the mixed or hybrid TTA type may have some rigid faces as well as some flexible faces. In general, this TTA type is composed by rigid faces and flexible faces comprising the cubical faces. Thereby, a mix of strain and stress-controlled interfaces might be expected, thus, combining both main advantages and disadvantages of each TTA types. In this scenario, works with rigid-rigid-flexible boundaries have been found such as Alshibli & Williams (2005),

<sup>#</sup>Corresponding author. E-mail address: dionatas@ufmt.br

<sup>1</sup>Universidade Federal de Mato Grosso, Barra do Garças, MS, Brazil.

<sup>2</sup>Universidade Federal do Rio Grande do Sul, Porto Alegre, RS, Brazil.

Submitted on November 15, 2021; Final Acceptance on March 24, 2022; Discussion open until August 31, 2022

<https://doi.org/10.28927/SR.2022.077321>



This is an Open Access article distributed under the terms of the Creative Commons Attribution License, which permits unrestricted use, distribution, and reproduction in any medium, provided the original work is properly cited.

AnhDan et al. (2005), Penumadu & Prashant (2005), Yin et al. (2009) and Hoyos et al. (2010). In addition, a rigid-flexible-flexible TTA boundary configuration can also be seen in works like Shibata & Karube (1965), Sutherland & Mesdary (1969), Lade & Duncan (1973), Lade (1978), Michelis (1988), Silvestri et al. (1988) and Kirkgard & Lade (2011). On the other hand, Sture & Desai (1979), Jamiolkowski et al. (1985), Arthur (1988), Sadek (2006) and Yin et al. (2009) have compared the aforementioned TTA types, describing the advantages and disadvantages of each one.

Therewith, the current paper aims to present a laboratory manufactured TTA. The manufactured TTA described hereafter was developed in the Laboratory of Geotechnical and Geoenvironmental Engineering at the Federal University of Rio Grande do Sul and comprises a mixed or hybrid TTA stress controlled. In this case, the manufactured TTA was set with three flexible faces and three rigid or fixed faces. Nonetheless, on the contrary of some previous works, these rigid faces do not move against the soil sample, serving only as a reaction frame against the flexible face. Silvani (2017) and Silvani et al. (2022) have already reported a similar TTA design, which has been adopted in order to avoid some sample translation movement. Summarizing, the manufactured TTA developed herein might be applied to test ordinary soil samples including natural soils, stabilized soils and weak or lightly cemented rocks that possess a peak strength lower than 1 MPa.

## 2. The manufactured true triaxial components

The new manufactured True Triaxial Apparatus (TTA) is composed by the main hardware, namely, the data acquisition

device plus the actuation control, a cubical cell, rubber cushions and the monitoring and controlling software. Each TTA component will be described in the sequence. In a first view, Figure 1 depicts a succinct description of the whole TTA components. A user-computer interface (algorithm) was developed based on the LabVIEW® 2013 Software where the user is able to control the TTA. The specimens pressurizing system was made by two Actuator controller Arduinos (AcA), which are responsible for commanding three sets of stepper motors coupled to three manual precision pressure valves. Sample pressure state and displacement response are acquired by three Pressure Transducers (PT) and nine Linear Variable Differential Transducers (LVDT), respectively. In this case, each face or axis is composed by one PT and three LVDTs.

### 2.1 Cubic cell

The cubic cell was designed to test soils and weak rocks cubic samples, 100 mm edges, at a maximum applied pressure of 1MPa. It uses the same configuration of the work seen in Reddy et al. (1992) and Sadek (2006), however, instead of stainless steel, it was manufactured in aluminum and age treated. Each of its six faces openings are coupled with flexible or rigid caps. For the flexibles faces, a silicon rubber cushion is placed in direct contact with the sample and it is touched by a set of three LVDTs, which are fixed by a 3D plastic printed support that is bolted to the “top hat” cap. The sealing is made through the straining of the cushion between the “top hat” and the cubic cell. In the opposing end of the cap, three holes were made to install the pressure transducer, the air supply and the wiring of the LVDTs. On each opposing face of the flexible faces, a rigid cap was placed as a reaction to the pressure applied in the cushions/sample.

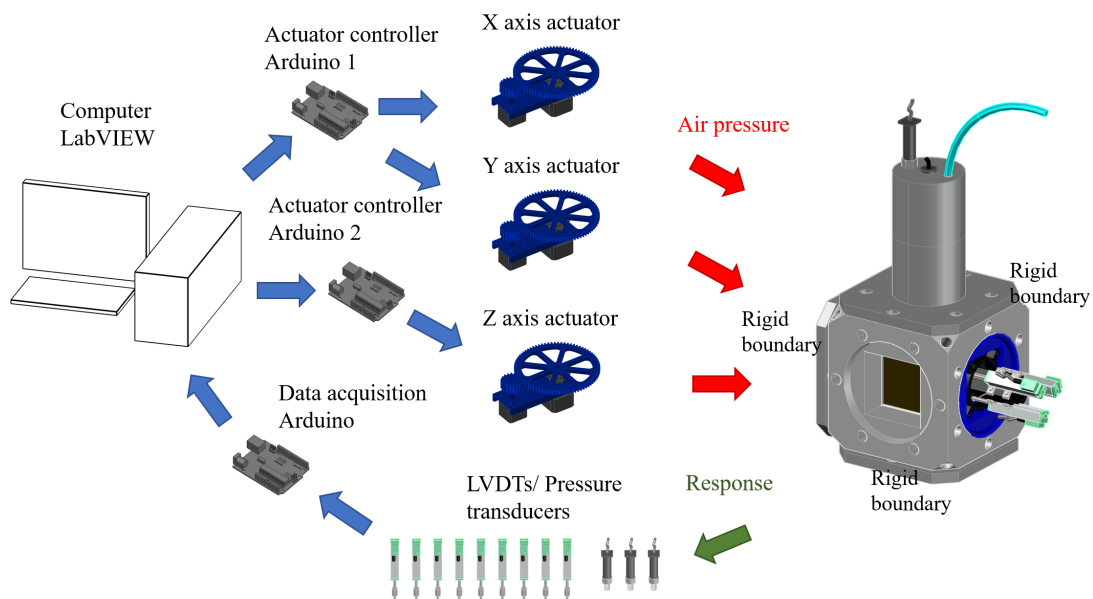


**Figure 1.** TTA schematic.

In two opposing corners of the cell cube drainage holes were drilled to enable water percolation and to release any generated pore pressure during the test and, in future developments, to allow the control of back pressure. On the other six corners of the cube, installation holes were drilled, that at the time of this work are not in use. An isometric view of the cell can be seen in Figure 2. In Figure 3, all the elements of the “top hat” cap are presented in a sliced view, where LVDTs wiring is omitted. In Figure 4, it is exhibited the LVDTs fixed in the support, the “top hat” and the assembled set. In Figure 5 an isometric view of the rigid cap is represented.

## 2.2 Silicon rubber cushions

The silicon rubber cushions were manufactured by the authors with Redelease's RX32 high resistance silicon rubber, utilizing 3% of the catalyzer provided by the manufacturer. The process consisted of weighting 300 g of the pre-polymer and 9 g of the catalyzer and mixing both components until homogeneity was achieved. The mixture was vacuumed for 15 min, while the mold was cleaned of any vestiges of previous cushion and an unmolding agent was sprayed over all surfaces. The mixture was poured in the mold the cap was bolted and the cushion was cured for 24 h. Afterwards, the cushion was removed from the mold and cured for six days until the full mechanical properties were achieved. In the fifth day, with a 3D printed template, small magnets were fixed with silicon glue aiming to facilitate the correct positioning of LVDTs fixating points as seen in Figure 6. The mold, cap and a finished cushion are presented in Figure 7. The mold and the cap were machined in aluminum and age treated.

## 2.3 Data acquisition and transducers

The bridge between the analog signal from the pressure transducers and LVDTs was provided by a digital converter. Three Adafruit ADS 1115 analog to digital converters were used. For greater noise control, each transducer had its own power supply, coupling LM7805 voltage regulators and 100  $\mu$ F capacitors. The digital signal was captured by an Arduino Nano microcontroller and sent to the computer via monitoring software. The communication between the Arduino and LabVIEW was made by serial port via USB. The LVDTs were purchased from Lemaq Automação. They are compatible with the Gefran PY-2-C-050, having 50 mm of course, potential difference output up to 5 V and infinite resolution. Coupled with the ADS 1115, the sensibility achieved in the LVDTs was 0,00152 mm, limited by the 15 bits resolution of the digital converter in single comparison. The PT purchased were Ashcroft k1 050 0-150 psi. When connected to the digital converter, they achieved the resolution of 0.5 kPa. All electronic components were purchased, but the circuit was manufactured, designed and Arduino coded by the authors. Figure 8 schematically presents the data acquisition system.

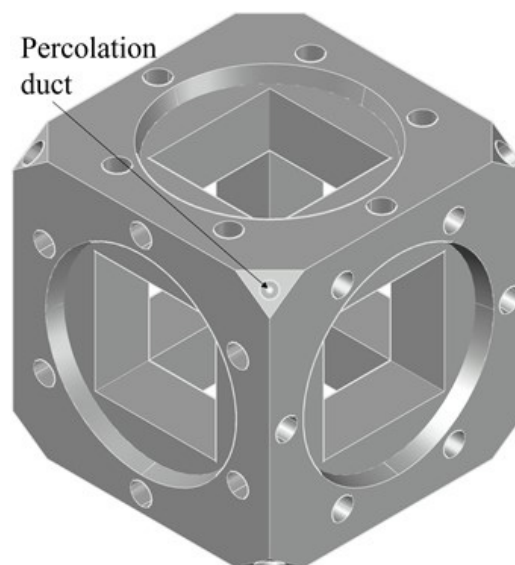


Figure 2. Cubic cell.

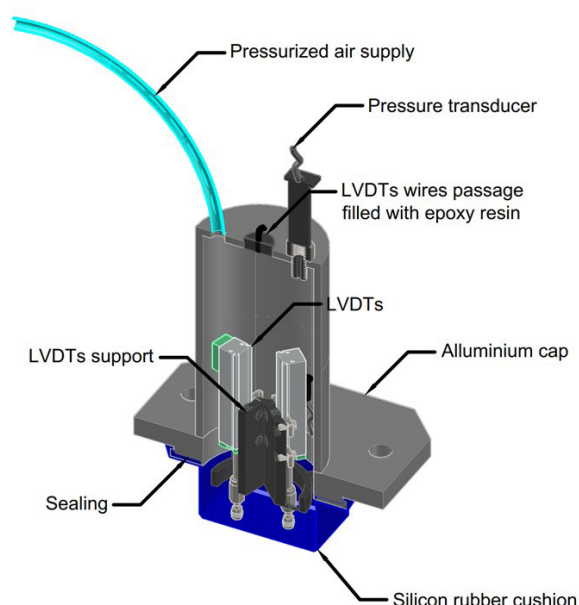
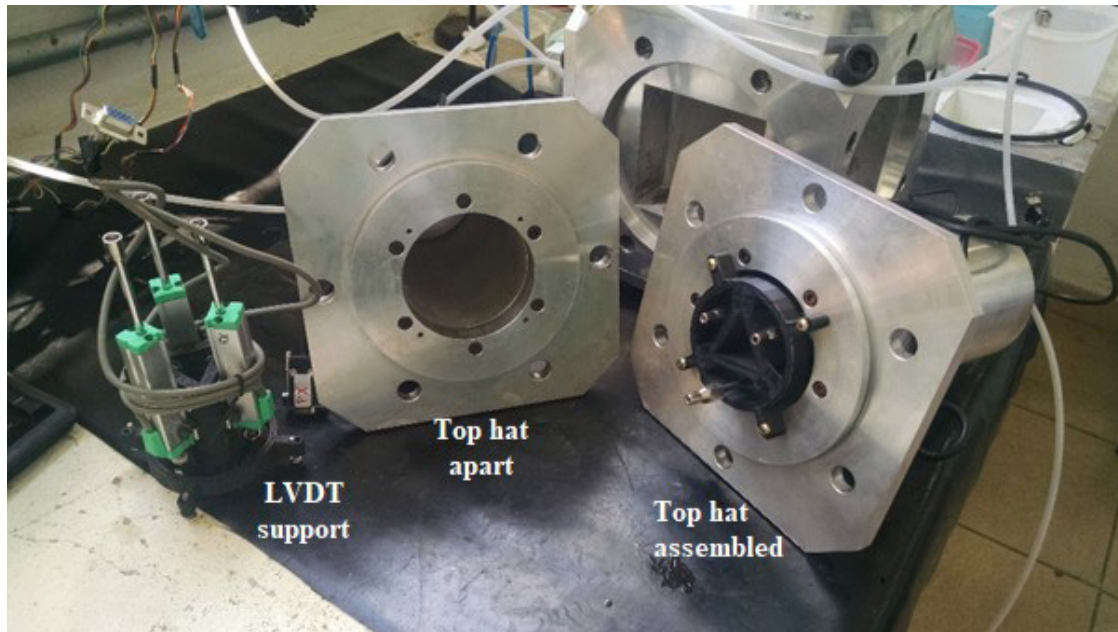


Figure 3. Sliced view of “top hat” cap.

## 2.4 Actuators

To control the compressed air pressure, three Norgren 11-018-110 precision pressure regulator valves were purchased. Those valves were coupled with NEMA 17 stepper motors with a pair of 3D printed gears and a base, enabling the automatic pressure control when the stepper motors were activated. The gears were fixed with epoxy resin in the handler of the valve and the stepper motor axis. All the described items are indicated in Figure 9.



**Figure 4.** LVDT support (left) and top hat apart (center) and assembled (right).

The gears ratio has both the function of increasing the torque and to decrease the revolution by step of the motors. Aiming to control them, two Arduino Uno microcontroller sets and L298 motor shield were purchased. To power the shield, an external computer power supply with 300 W and 12 V was used. Since each motor shield can be used to control up to two stepper motors, its required at least two Arduinos. The communication between the Arduinos and LabVIEW was achieved by a serial port via USB. All the 3D printing, design, assembly and coding were made by the authors and the electronics components were purchased. The total cost of device consisting of machining of the aluminum parts, electro-mechanic, hydraulic and transducers was around 6500 USD at purchased time.

### 2.5 Monitoring and controlling software

To perform the monitoring and controlling of the apparatus, a software was developed in LabVIEW. Since LabVIEW does not support natively the communication between itself and Arduino, the code was first needed to be written, since only some libraries with basic Arduinos functions as analog read or digital write are available. The final code was achieved using the serial communication protocol, so the computer could communicate with each Arduino using different serial ports. The proceeding modules were developed as consolidation and shearing.

## 3. Apparatus validation

To assess the performance of the apparatus, a series of tests was made. Two types of soils, with and without

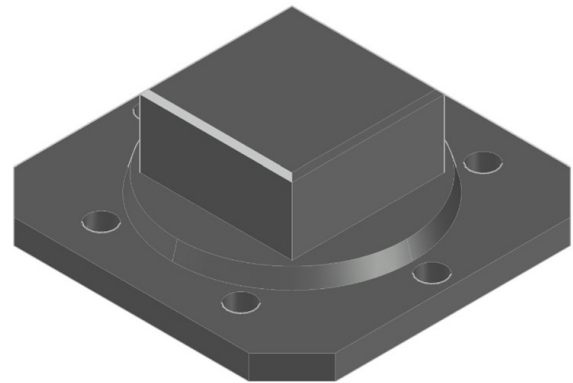


**Figure 5.** Rigid cap.

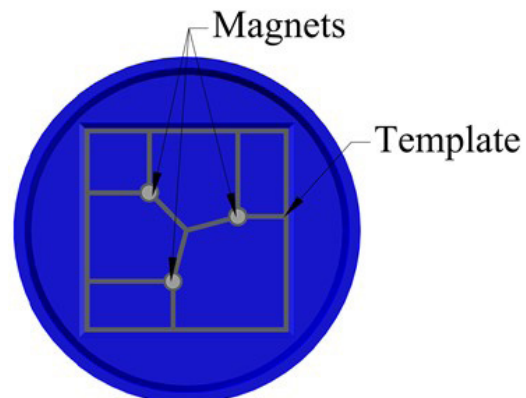


**Figure 6.** Magnets fixing template.



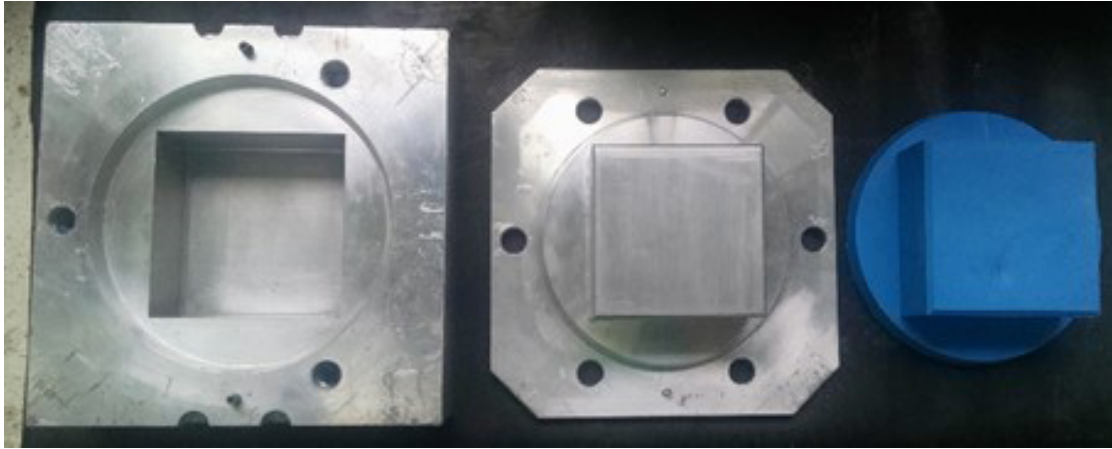


**Figure 7.** Mould (left), cap (center) and cushion (right).

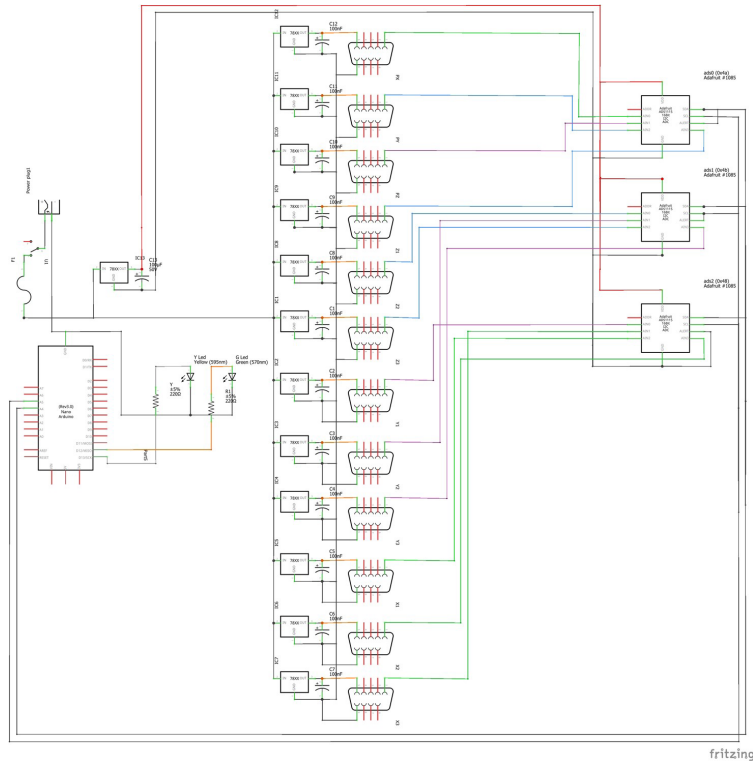


**Figure 8.** Data acquisition schematic.

cement addition, were tested in the developed TTA and in a conventional ST aiming to compare and validate the new apparatus.

### 3.1 Uniform fine sand

The first investigated soil was Osorio sand, extracted from a city near Porto Alegre, in southern Brazil. It was classified as a non-plastic uniform fine sand (SP), with specific gravity

of the solids of 2.65. The mineralogical analyses shown that the sand composition was predominantly quartz. The mean diameter ( $D_{50}$ ) was 0.250 mm and the uniformity ( $C_u$ ) and curvature ( $C_c$ ) were 2.11 and 1.15, respectively. The minimum and maximum void ratios were 0.60 and 0.90. The soil characterization was presented by Marques et al. (2021).

To set the sample inside the cubic cell, two additional caps were 3D printed and all rigid caps were bolted in place, remaining only the top face opened, as seen in Figure 10.

All the inside faces of the cube were lubricated with vaseline to avoid shearing transfer. The soil was then mixed with distilled water, aiming the moisture content of 10% and a relative density of 50%. These parameters were defined to compare the results with the ones of Consoli et al. (2009). The mixture was then placed in the center of the cell and compacted in three layers until the 100 mm height was achieved. After that, the two printed caps were removed, all the cushions were lubricated in all external surface that touched the sample or the cubic cell, and all the “top hats” were bolted in place.

With the moulded sample in place, the software-controlled step proceeded. To inundate the sample, 30 kPa of confining pressure was applied and at least two time the void volume was percolated with ascendant flow of distilled water. Afterwards the sample was confined to consolidation pressures of 50, 75 and 100 kPa. The shearing, considering Lode angle  $0^\circ$ , was performed increasing the pressure in the vertical axis and reducing the pressure in both horizontal axes, maintaining the same mean stress, at an increase rate of 2 kPa/

min in the vertical axis and at a decrease rate of 1 kPa/min in the horizontal axis until the failure of the sample was observed. The obtained results are presented in the Figure 11.

The obtained friction angle of  $38.4^\circ$  was compared with the  $37^\circ$  achieved in Consoli et al. (2009). The difference can be the result of the different type of test, strain-controlled vs stress controlled, distinct geometry of sample, cubical of 100 mm of edge opposing to cylindrical 100 mm of diameter and 200 mm of height as seen in Ferreti (2012), Lan et al. (2018), Tripura & Das (2017) or the natural material variability.

### 3.2 Cemented uniform fine sand

To further validate the apparatus, tests with cemented sand were performed in the TTA and the ST. The Osorio sand, same as utilized in the previous experiment, was mixed with high initial strength Portland cement (Type III), with specific gravity of 3.15. The samples were moulded with moisture content of 8.5%, cement content of 3.3% by of dry sand, and a target dry density of  $15.0 \text{ kN/m}^3$ . Cylindrical specimens with 100 mm diameter and 200 mm height were moulded for ST tests and cubical specimens with 100 mm edges were prepared for TTA tests. The process of mixture and moulding was made in 1h or less, lower than the cement setting time of 3.25 h. The moulded samples were placed in polypropylene bags to maintain the moisture content and proceeded to a humid room with temperature within  $23 \pm 2^\circ \text{C}$  and relative humidity above 95%. The samples were maintained in the humid room for six days and, in the seventh day, tested. The sample acceptance was a 1% of deviance in dry density and dimensions and 0.5% in moisture content.

The tests were performed following the procedure described in the previous test, except that for the ST tests the samples were back pressured with 300 kPa and Skempton  $B$  parameter higher than 0.99. During shearing, both apparatuses performed an increase of the vertical pressure, with a rate of 2 kPa/min, and the mean stress were maintained by reducing either the confining pressure or the horizontal pressures, with

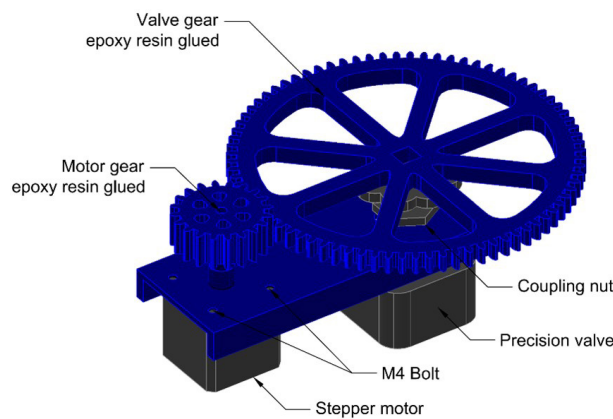


Figure 9. Pressure control actuators.

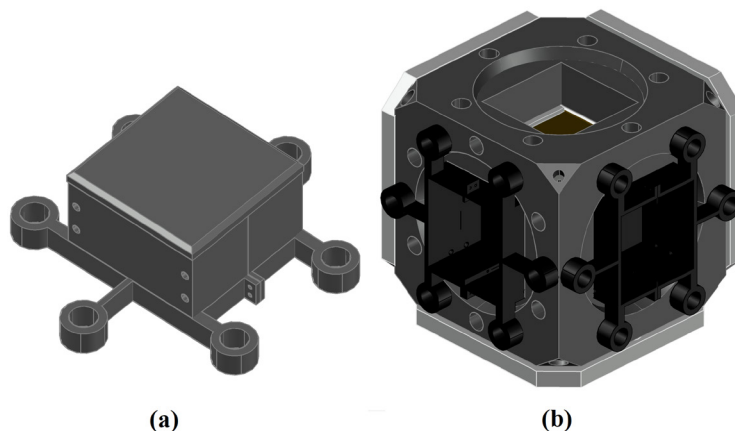


Figure 10. (a) 3D printed cap; (b) sample positioning.

a rate of 1 kPa/min. For the ST, three samples were tested under the confining pressures of 50, 100 and 200 kPa. For the TTA, nine tests were performed, three under 50 kPa, two under 75 kPa, two under 100 kPa, one under 125 kPa and one under 150 kPa of confining pressure. The tests were finished when the strain was observed without a significative stress.

The ST tests resulted in a friction angle of  $33.6^\circ$  and a  $c'$  of 3.3 kPa, while the TTA tests resulted in a friction angle of  $34.3^\circ$  and a  $c'$  of 8.4 kPa (Figure 12). These differences can be derived from either the geometry of the samples and/or natural material variability. Similar results were observed in the works of Reddy & Saxena (1993).

### 3.3 Cemented clayey sand

To further validate the TTA, a battery of tests involving Botucatu residual soil, a clayed sand described also in the work of Consoli et al. (2018). The same mold and acceptance criteria from the previous tests were utilized. The moisture content targeted this time was 10% and a dry density of

$14.6 \text{ kN/m}^3$  and 1.07% by mass of dry soil of type III Portland cement. The same curing procedure was performed, with two days of curing in climate-controlled room and in the third day the test were performed.

A total of four samples were tested, two in TTA and two in ST, with 100 and 150 kPa consolidation pressures. For the TTA, the ending of the tests was characterized by the rupture of the cushion, while for the ST the high strain without an increase of the stress were noted. The results of those tests can be seen in Figure 13. A fair agreement of the results from the different apparatuses can be observed. The small difference in the results could be attributed to distinct local strain measurements systems: Hall effect transducers for ST tests and LVDTs for TTA tests.

### 3.4 Uniform sand under TTA

The last tests set was performed utilizing the same Osorio sand and the same procedures described in item 3.1. To fully assess the apparatus capacity, a full rosette was developed, utilizing the angles of  $0, 30, 60, 90, 120, 150$  and  $180^\circ$  between  $\sigma_z$  and the loading path in the octahedral plane, all under the same mean stress of 100 kPa (Figure 14.). In Figure 15, it is exhibited the performance of the samples in the previous tests, with the stress strain behaviour.

The results demonstrated a certain level of anisotropy in the material, potentially caused by the specimens' preparation method, and an internal consistency of the results. When comparing the results of Lode angles  $0$  and  $120^\circ$ , the first shows a higher stress then the second. The same can be seen for  $30$  and  $150^\circ$  and also for  $60$  and  $180^\circ$ . Those results correspond to the same type of tests, axial compression, simple shear and axial extension, but with a different alignment with the compaction axis. Overall, the tests shown a low noise level and consistency.

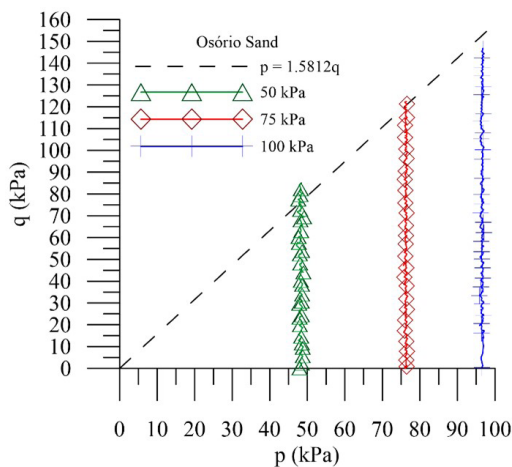


Figure 11. Shear response of Osorio Sand.

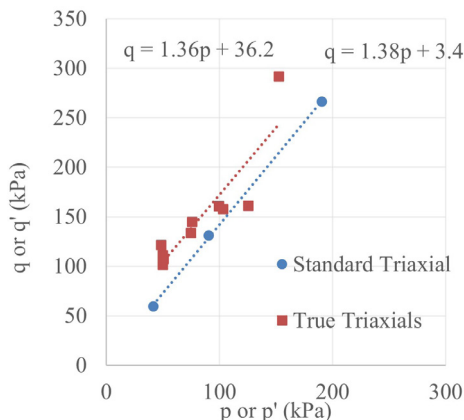


Figure 12. Cemented Osorio sand response.

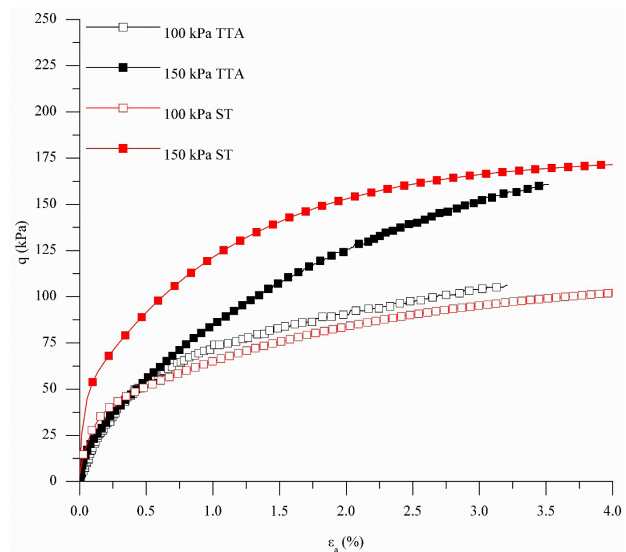


Figure 13. TTA vs ST of cemented Botucatu clayey sand.

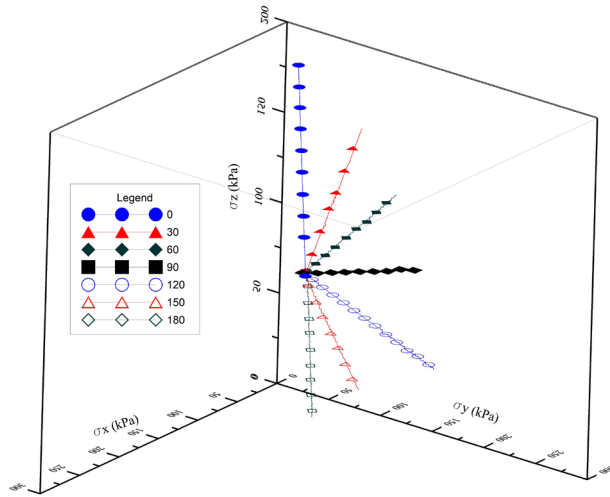


Figure 14. Uniform sand stress rosette.

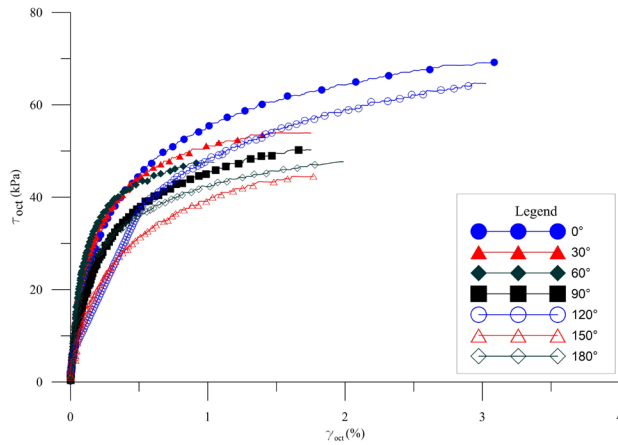


Figure 15. Stress strain behavior of uniform sand under TTA.

## 4. Conclusion

This paper reported a successful and affordable development of an automated true triaxial apparatus. The TTA main components were based on open source tools, which enabled the production of an accessible and effective equipment. The manufactured true triaxial test results exhibited well agreement when compared to other test results from other testing equipment, such as a well validated standard triaxial apparatus. Anisotropy in Osorio sand was observed.

## Acknowledgements

The authors wish to explicit their appreciation to FAPERGS/CNPq 12/2014 – PRONEX (grant # 16/2551-0000469-2), MCT-CNPq (INCT, Universal & Produtividade em Pesquisa) and MEC-CAPES (PROEX) for the support to the research group.

## Declaration of interest

The authors declare that no conflict of interest to disclose by this paper.

## Authors' contributions

Dionatas Hoffmann Andreghetto: Conceptualization, Investigation, Hardware, Software, Data curation, Visualization, Writing – original draft. Lucas Festugato: Conceptualization, Data curation, Methodology, Supervision, Validation, Writing – review & editing, Funding acquisition, Resources. Gustavo Dias Miguel: Formal Analysis, Investigation, Methodology, Writing – review & editing. Andressa da Silva: Writing – review & editing.

## List of symbols

$p$	Mean Stress
$q$	Deviatoric stress ( $\sigma_1 - \sigma_3$ )
$AcA$	Actuator controller Arduinos
$C_s$	Coefficient of curvature
$C_u$	Coefficient of uniformity
$D_{50}$	Mean diameter
$LVDT$	Linear Differential Transducer
$PT$	Pressure Transducers
$ST$	Standard Triaxial
$TTA$	True Triaxial Apparatus
$\epsilon_a$	Axial strain
$\gamma_{oct}$	Distortional strain in octahedral plane
$\sigma_x$	Horizontal stress x
$\sigma_y$	Horizontal stress y
$\sigma_z$	Vertical stress z
$\tau_{oct}$	Shear stress in octahedral plane

## References

- Airey, D.W., & Wood, D.M. (1988). The cambridge true triaxial apparatus. In R. Donaghe, R. Chaney, and M. Silver, (Eds.), *Advanced triaxial testing of soil and rock, ASTM STP 977* (pp. 796). ASTM International.
- Alshibli, K.A., & Williams, H.S. (2005). A true triaxial apparatus for soil testing with mixed boundary conditions. *Geotechnical Testing Journal*, 28(6), 534-543.
- AnhDan, L. Q., Koseki, J., Hayano, K., & Sato, T. (2005). True triaxial apparatuses with two rigid boundaries, site characterization and modeling (GSP138). In *Geo-Frontiers Congress*. Austin, Texas, GeoInstitute of ASCE.
- Arthur, J.R.F. (1988). State-of-the-art paper: cubical devices: versatility and constraints, advanced triaxial testing of soil and rock. In R.T. Donaghe, R.C. Chaney, and M.L. Silver (Eds.), *ASTM STP 977* (pp. 743). ASTM International.



- Choi, C., Arduino, P., & Harney, M.D. (2008). Development of a true triaxial apparatus for sands and gravels. *Geotechnical Testing Journal*, 31(1), 32-44.
- Consoli, N.C., Festugato, F., & Heineck, K.S. (2009). Strain-hardening behaviour of fibre-reinforced sand in view of filament geometry. *Geosynthetics International*, 16(2), 109-115.
- Consoli, N.C., Winter, D., Leon, H.B., & Scheuermann Filho, H.C. (2018). Durability, strength, and stiffness of green stabilized sand. *Journal of Geotechnical and Geoenvironmental Engineering*, 144(9), 04018057.
- Ferreti, E. (2012). Shape-effect in the effective laws of plain and rubberized concrete. *CMC Tech Science Press*, 30(3), 237-248.
- Hambly, E.C. (1969). A new true triaxial apparatus. *Geotechnique*, 19(2), 107-124. <http://dx.doi.org/10.1680/geot.1969.19.2.307>.
- Hoyos, L.R., Perez-Ruiz, D.D., & Puppala, A.J. (Feb 20-24, 2010). A refined true triaxial cell for modeling unsaturated soil response under suction controlled stress paths. In *GeoFlorida 2010: Advances in Analysis, Modeling and Design*, Orlando, Florida, Reston, VA: ASCE, pp. 381-389.
- Ibsen, L.B., & Praastrup, U. (2002). The danish rigid boundary true triaxial apparatus for soil testing. *Geotechnical Testing Journal*, 25(3), 1-12.
- Ismail, M.A., Sharma, S.S., & Fahey, M. (2005). A small true triaxial apparatus with wave velocity measurement. *Geotechnical Testing Journal*, 28(2), 1-10.
- Jamiolkowski, M., Ladd, C.C., Germaine, J.T., & Lancellotla, R. (Aug 12-16, 1985). New developments in field and laboratory testing of soils. In *Proceedings of the 11th International Conference on Soil Mechanics and Foundation Engineering* (Vol. 1, pp. 57-153). San Francisco. Rotterdam, The Netherlands: A. A. Balkema.
- Kirkgard, M.M., & Lade, P.V. (2011). Anisotropic three dimensional behavior of a normally consolidated clay. *Canadian Geotechnical Journal*, 30(5), 848-858.
- Ko, H.Y., & Scott, R.F. (1967). A new soil testing apparatus. *Geotechnique*, 17(1), 40-57.
- Lade, P.V. (1978). Cubical triaxial apparatus for soil testing. *Geotechnical Testing Journal*, 1(2), 93-101.
- Lade, P.V., & Duncan, J.M. (1973). Cubical triaxial tests on cohesionless soil. *Journal of the Soil Mechanics and Foundations Division*, 99(10), 793-812.
- Lan, G., Wang, Y. & Chao, S. (2018). Influences of specimen geometry and loading rate on compressive strength of unstabilized compacted earth block. *Advances in Materials Science and Engineering*, 2018, 5034256. <https://dx.doi.org/10.1155/2018/5034256>.
- Marques, S.F.V., Festugato, L., & Consoli, N.C. (2021). Stiffness and strength of an artificially cemented sand cured under stress. *Granular Matter*, 23, 35. <http://dx.doi.org/10.1007/s10035-021-01099-1>.
- Matsuoka, H., Sun, D., Kogane, A., Fukuzawa, N., & Ichihara, W. (2002). Stress-strain behaviour of unsaturated soil in true triaxial tests. *Canadian Geotechnical Journal*, 39(3), 608-619.
- Michelis, P. (1988). A true triaxial cell for soil and rock. In R.T. Donaghe, R.C. Chaney and M.L. Silver (Eds.), *Advanced Triaxial Testing of Soil and Rock, ASTM STP 977*. American Society for Testing and Materials, pp. 806-818.
- Penumadu, D., & Prashant, A. (Jan 24-26, 2005). Automated flexible boundary true triaxial system for cohesive soils, site characterization and modeling (GSP138). In *Geo-Frontiers Congress 2005*, Austin, TX, Reston, VA: Geo-Institute of ASCE.
- Reddy, K. R. & Saxena, S. K. (1993). Effects of cementation on stress-strain and strength characteristics of sands. *Soils and Foundations*, 33(4), 121-135.
- Reddy, K.R., Saxena, S.K., & Budiman, J.S. (1992). Development of a triaxial testing apparatus. *Geotechnical Testing Journal*, 15(2), 89-105.
- Sadek, T. (2006). *The multiaxial behaviour and elastic stiffness of hostun sand* [Doctorship thesis, University of Bristol]. University of Bristol Repository.
- Shibata, T., & Karube, D. (Sept 8-15, 1965). Influence of the Variation of the Intermediate Principal Stress on the Mechanical Properties of Normally Consolidated Clays. In *Proceedings of the 6th International Conference on Soil Mechanics and Foundation Engineering* (Vol. 1, pp. 359-363). Montreal, Canada. Toronto: University of Toronto Press.
- Silvani, C. (2017). *Artificially cemented soil tested in a cubical cell: isotropy at small strains and at failure* [Doctoral Thesis, Federal University of Rio Grande do Sul]. Lume digital repository <https://lume.ufrgs.br/handle/10183/157899> (in Portuguese).
- Silvani, C., Ibraim, E., Scheuermann Filho, H.C., Festugato, L., Diambra, A., & Consoli, N.C. (2022). Sand-fly ash-lime blends: mechanical behaviour under multiaxial stress condition. *Journal of Materials in Civil Engineering*, [ahead of print].
- Silvestri, V., Yong, R.N., & Mohamed, A.M.O. (1988). A true triaxial testing cell, advanced triaxial testing of soil and rock. In ASTM International. *ASTM STP 977* (pp. 819-833). ASTM International.
- Sivakugan, N., Chameau, J. L., Holtz, R. D., & Altschaeffl, A. G. (1988). Servo-controlled cuboidal shear device. *Geotechnical Testing Journal*, 11(2), 119-124.
- Sture, S., & Desai, C.S. (1979). Fluid cushion truly triaxial or multi-axial testing device. *Geotechnical Testing Journal*, 2(1), 20-33.
- Sutherland, H.B., & Mesdary, M.S. (Aug 25-29, 1969). The influence of the intermediate principal stress on the strength of sand. In *Proceedings of the 7th International Conference on Soil Mechanics and Foundation Engineering* (Vol. 1, pp. 391-399). Mexico City, Sociedad Mexicana de Mecanica.

- Tripura, D. D. & Das, S. (2017). Shape and size effects on the compressive strength of cement stabilised rammed earth. *AEI 2017: Resilience of the Integrated Building*, 1210-1217. <https://doi.org/10.1061/9780784480502.028>.
- Yin, J.H., Cheng, C.M., Kumruzzaman, M., & Zhou, W.H. (2009). New mixed boundary, true triaxial loading device for testing three-dimensional stress-strain strength behavior of geomaterials. *Canadian Geotechnical Journal*, 47(1), 1-15.